Dalton Transactions



PAPER

View Article Online
View Journal | View Issue



Cite this: *Dalton Trans.*, 2023, **52**, 11535

Effect of bromine substitution on blue phosphorescent *trans-*(N-heterocyclic carbene) Pt(II) acetylide complexes†

Amran A. T. Khan, Habtom B. Gobeze, Tanjila Islam, Hadi D. Arman and Kirk S. Schanze *

N-heterocyclic carbene complexes of the type *trans*-(NHC)₂Pt^{II}(C≡C-Ar)₂ (where Ar = phenyl or substituted phenyl) are of interest as violet and blue phosphors. These complexes emit efficient phosphorescence in solution and in the solid state, and they have been applied as phosphors in organic light emitting diodes. This study explores the effect of bromine substitution on the *trans*-(NHC)₂Pt^{II}(CC-Ar)₂ chromophore through photophysical studies of a pair of complexes in which the phenyl groups feature either 3,5-dibromo- or 4-monobromo-substituents (**IPt-DB** and **IPt-MB**, respectively). The Br atoms were introduced as heavy atom(s) with the aim to enhance spin-orbit coupling and increase the radiative and non-radiative decay rates of the phosphorescent triplet state. Both **IPt-MB** and **IPt-DB** exhibit sky-blue phosphorescence in solution and in PMMA matrix. Interestingly, the emission quantum yield and lifetime of **IPt-MB** are substantially lower compared to **IPt-DB** in solution. This effect is attributed to a substantially larger non-radiative decay rate in the mono-bromo complex. Analysis of the photophysical data, combined with DFT and TD-DFT calculations, suggest that the difference in photophysical properties of the two complexes is related to the position of the Br-substituents on the phenyl acetylide rings. In short, in **IPt-MB**, the Br-substituents are located *para*-to the Pt-CC-unit, and this gives rise to stronger electron-vibrational coupling in the excited state, enhancing the rate of non-radiative decay.

Received 18th May 2023, Accepted 17th July 2023 DOI: 10.1039/d3dt01483e

rsc.li/dalton

Introduction

Transition metal complexes with π -conjugated ligands have long been studied for their rich photophysical properties and applications in sensing, photocatalysis, artificial photosynthesis, photodynamic therapy, optoelectronics, and non-linear optics. ^{1,2} One of their advantages is that the transition metal can introduce heavy atom induced spin-orbit coupling (SOC) which enhances the probability of spin-forbidden transitions. As a result, transition metal complexes often feature efficient luminescence from the triplet manifold and relatively short triplet lifetimes due to enhanced radiative and non-radiative decay rates. ^{3,4}

Luminescent transition metal complexes that contain N-heterocyclic carbene (NHC) ligands have recently received significant attention. $^{5-7}$ NHC ligands are strong σ -donors that can reduce the efficiency of non-radiative decay by limiting the

Department of Chemistry, University of Texas at San Antonio, One UTSA Circle, San Antonio, TX 78249, USA. E-mail: kirk.schanze@utsa.edu

†Electronic supplementary information (ESI) available. CCDC 2263726 and 2263727. For ESI and crystallographic data in CIF or other electronic format see DOI: https://doi.org/10.1039/d3dt01483e

rate of thermally activated crossing to non-emissive metal centered (d-d) excited states.^{8,9} To date, a variety of NHC metal complexes based on Ir(III), Ru(II), Pt(II), Pd(II), Ag(I), and Cu(I) have been reported.^{5,6,10} These complexes exhibit interesting and useful luminescence properties owing to their wide variety of structural designs, long emission lifetimes, high radiative rates, tunable excited state energies, and large Stokes shifts.⁸

Platinum(II)-NHC complexes with a variety of π -conjugated ligands have been widely investigated owing to their remarkable photophysical properties. These complexes have been subjected to various structural modifications aimed at finetuning their emission energies and optimizing their emission efficiency. 11-13 In particular, Pt(II)-NHC complexes that contain aryl acetylide ligands (e.g., Ar-C≡C-) have been investigated extensively due to their good air and thermal stability and the ability to tune their excited state energies and lifetimes. 9,14-19 The design principle behind these complexes includes utilizing the Pt(II) as heavy metal to induce SOC which maximizes the use of both singlet and triplet excited states which are primarily localized on the aryl acetylide ligands. 18,20,21 Venkatesan and co-workers first reported complexes of the type, cis- and trans-(NHC)₂Pt(C≡C-Ar)₂ in which the structure and substituents on the aryl acetylide ligands were Paper **Dalton Transactions**

varied. 9,14,15 All the compounds were emissive both in solution and the solid state, and some of the complexes showed strong blue emission with relatively high quantum yields. A few years later our group reported an improved synthesis of trans-(NHC)₂Pt(C=C-Ar)₂ complexes and leveraged the synthetic strategy to construct a series of novel complexes with efficient visible phosphorescence and strong triplet-triplet absorption that could be applied in non-linear absorption.¹⁷

A key application of strongly luminescent transition metal complexes is as phosphors for organic light emitting diodes (PHOLEDs). Considerable effort has been made to develop efficient deep blue luminescent metal complexes, and to utilize them as phosphors in PHOLEDs with high external quantum efficiency (EOE). 16,22-28 However, developing complexes that give rise to "true" deep blue luminescence while maintaining high quantum efficiency remains a challenge.²⁹ (Deep blue is typically defined as emission with CIE coordinates (0.14, 0.08).²⁷) As a result, despite the success of red and green PHOLEDs, deep blue PHOLEDs with high EQE are still rare.25 For example, Ir(III) based commercially available red and green emitters can reach up to 100% internal quantum efficiency (IQE) and ~25% EQE, whereas PHOLEDs with deep blue phosphors still suffer from lower efficiency and relatively short device lifetimes.30 Another limitation associated with some phosphors is that their relatively long lifetimes cause device efficiency roll-off due to triplet-triplet annihilation and triplet-polaron quenching. 29,31

In previous work, we reported the NHC-Pt(II) complex NPtPE1 (Chart 1) which features a deep blue phosphorescence with a moderate quantum efficiency. NPtPE1 was used as a phosphor in a vapor deposited OLED which displayed a peak EOE of 8%. 19,32 However, the triplet state lifetime of **NPtPE1** is relatively long (~10 μs in the solid state), which contributed to efficiency roll-off at higher current density in the OLED. In an effort to tune the trans-(NHC)₂Pt(C=C-R)₂ chromophore to maintain the efficient deep blue emission, but reduce the triplet lifetime, we designed two bromine substituted congeners, IPt-MB and IPt-DB (Chart 1). The Br-atoms were introduced into these structures with the aim to increase spin-orbit coupling in the excited states, with the notion that this might increase both the emissive triplet state radiative and non-radiative decay rates (k_r and k_{nr} , respectively), reducing the lifetime, but potentially to retain a moderately efficient phosphorescence efficiency.33-36

$$R_1 \xrightarrow{R_2} Cy \xrightarrow{Cy} N \xrightarrow{R_2} Cy$$

$$R_2 \xrightarrow{Cy} Pt \xrightarrow{R_2} R_2$$

$$R_2 \xrightarrow{Cy} R_2$$

NPtPE1: $R_1 = H$, $R_2 = H$ $R_1 = Br, R_2 = H$ IPt-DB: $R_1 = H, R_2 = Br$ IPtPCF₃: $R_1 = CF_3$, $R_2 = H$

Chart 1

This paper reports a detailed structural and photophysical characterization of IPt-MB and IPt-DB providing a comparison with previously studied trans-(NHC)₂Pt(C≡C-R)₂ chromophores. The results show that the inclusion of the two Bratoms in IPt-DB has very little effect on the photophysical parameters. By contrast, the single Br-atom in IPt-MB elicits a profound effect on the non-radiative decay rate, leading to a substantially reduced lifetime, but disappointingly also a diminished phosphorescence quantum yield. The difference in the effect of the Br-atoms in the two complexes is attributed to positional dependence on their involvement in the frontier orbitals that dominate the electronic transitions to the lowest excited states.

Results and discussion

Synthesis and structural characterization

The precursor compounds 1-bromo-4-ethynylbenzene (1) and 1,3-dibromo-5-ethynylbenzene (2) were synthesized Sonogashira coupling followed by a deprotection reaction (Scheme S1†). 37,38 The precursor NHC complex (Im), PtCl₂ (5, Scheme S2†) was obtained by a one-pot synthesis that was previously reported, through an in situ formed Ag(1)-NHC complex followed by transmetalation with K2PtCl4.18 Compounds IPt-MB and IPt-DB were synthesized by a Hagihara coupling reaction, in which the aryl acetylide ligand was introduced (Scheme S2†).39,40 IPt-MB and IPt-DB were characterized by ¹H-NMR, ¹³C-NMR and X-ray crystallography, mass spectrometry and elemental analysis (ESI section†).

X-ray crystallography confirmed the *trans* stereochemistry of both complexes (Fig. 1). Selected bond lengths and angles are shown in Table 1, and the detailed crystallographic data are reported in the ESI.† As expected, the Pt atom resides on the inversion center of both complexes. Pt-Ccarbene bond lengths of IPt-MB and IPt-DB are 2.025 Å and 2.029 Å, respectively, whereas Pt-C_{sp} bond lengths are found to be 2.009 Å and 2.001 Å, respectively. Both types of bond lengths are very similar to the prior reported trans-(NHC)Pt(II) acetylide complexes. The $C_{carbene}$ -Pt- C_{sp} bond angles were 89.21° and 89.8° for **IPt-MB** and **IPt-DB**, respectively.

Photophysical properties

The absorption and emission spectra of the complexes were recorded in THF solution, and they are shown in Fig. 2. Both complexes showed similar absorption spectra with bands near 310 nm and 285 nm. These absorption bands are predominantly based on π - π * transitions of the phenyl acetylide ligands. 18,20,41,42

IPt-MB and **IPt-DB** feature sky blue emission with λ_{max} = 456 and 458 nm, respectively, with a shoulder at 480 nm due to vibronic coupling.41 The emission spectra of IPt-MB and IPt-DB are red-shifted approximately 15 nm (~640 cm⁻¹) compared to the parent complex NPtPE1. The red-shift is apparently because of the electron withdrawing effect of the -Br substituents. However, despite having similar emission spectra

Dalton Transactions Paper

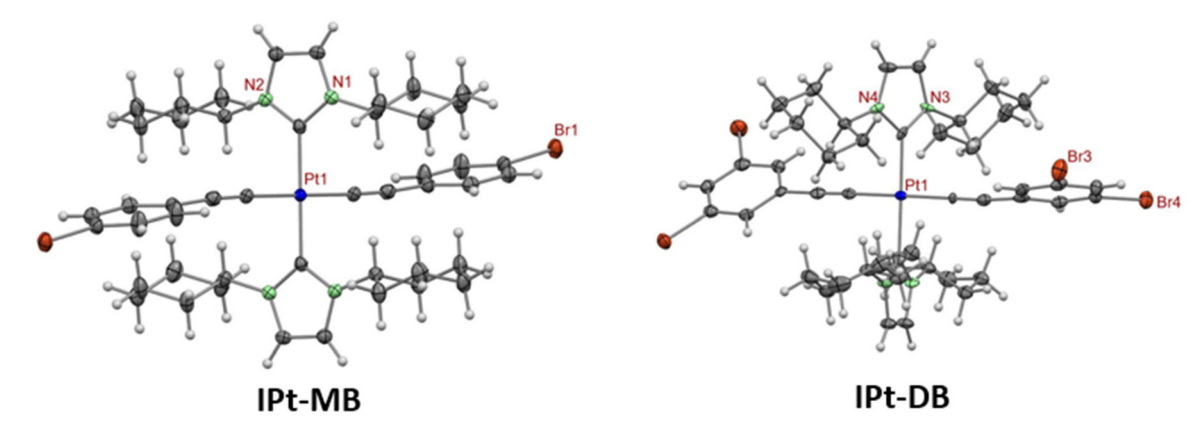


Fig. 1 ORTEP diagrams for IPt-MB and IPt-DB, with ellipsoid at the 50% probability level. Carbon atoms are shown in grey, and hydrogen atoms are shown in light grey. Solvent molecules were removed for clarity.

Table 1 Selected bond lengths and dihedral angles from X-ray crystal structures

	Bond length (Å)			Bond angle (°)		
	Pt-C _{Carbene}	$Pt-C_{sp}$	C≡CPh	N-carbene-N	$C_{Carbene}$ -Pt- C_{sp}	
IPt-MB IPt-DB	Pt1-C1: 2.025(3) Pt1-C1: 2.029(6) Pt1-C6: 2.035(6)	Pt1-C16: 2.009(3) Pt1-C31: 2.001(7) Pt1-C39: 1.983(7)	C16-C17: 1.200(5) C31-C32: 1.222(11) C39-C40: 1.216(11)	N1-C1-N2: 105.0(3) N1-C1-N2: 105.4(5) N3-C16-N4: 105.3(5)	C1-Pt1-C16: 89.21(12) C1-Pt1-C39: 89.8(3) C1-Pt1-C31: 89.6(3) C16-Pt1-C39: 90.6(3) C16-Pt1-C31: 90.0(3)	

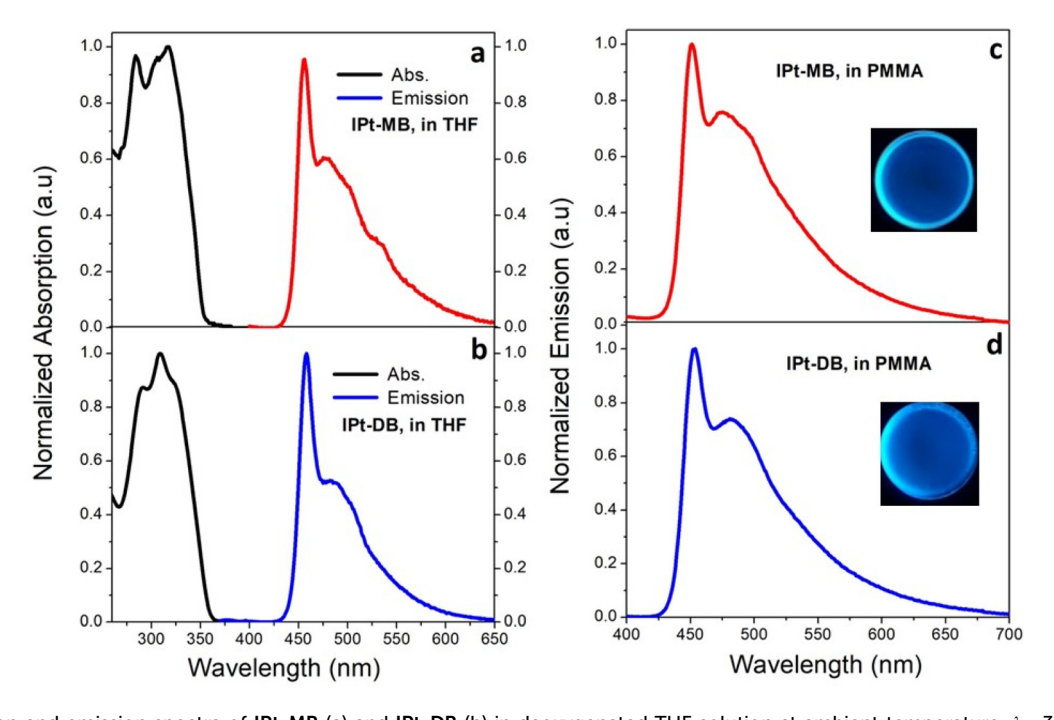


Fig. 2 Absorption and emission spectra of IPt-MB (a) and IPt-DB (b) in deoxygenated THF solution at ambient temperature, λ_{ex} 330 nm. Emission spectra of IPt-MB (c) and IPt-DB (d) in PMMA matrix.

and energies, IPt-MB and IPt-DB showed distinct differences in emission quantum yield, lifetime, and radiative and nonradiative decay rates. In particular, as shown in Table 2, in the THF solution, the emission quantum yield and lifetime are substantially greater for IPt-DB compared to IPt-MB. The emission quantum yields for the two complexes differ by more Paper **Dalton Transactions**

Table 2 Photophysical properties in THF solution

Compound	$\lambda_{\max}^{(abs)}/$ nm	$\lambda_{\max}^{(\mathrm{em})}/$ nm	$\Phi_{ m em}$	τ _{em} / μs	$\frac{k_{\rm r}^{\ a}/10^4}{{ m s}^{-1}}$	$\frac{k_{\rm nr}^{\ a}}{10^4}$ s ⁻¹	E _{em} / eV
IPt-MB	316	456	0.02	0.39	5.13	250	2.71
IPt-DB	309	458	0.2	7.59	2.64	11	2.71
IPtPCF ₃ ^b	310	452	0.19	5	3.8	16	2.74
$NPtPE1^b$	279	444	0.03	1.7	1.8	57	2.79

^a Calculated using the equations: $k_r = \Phi_{PL}/\tau_{PL}$ and $k_{nr} = (1/\tau_{PL}) - k_r$, where $\tau_{\rm PL} = \langle \tau \rangle$. Data from ref. 18.

than 10-fold, and the lifetime of IPt-DB is 20-fold larger than that of IPt-MB (Fig. S13 and S14†). The radiative and nonradiative decay rates (k_r and k_{nr} , respectively) are computed from the photophysical parameters. Here it is seen that k_r values for the two complexes are similar; however, $k_{\rm nr}$ is 25-fold greater for IPt-MB compared to IPt-DB.

In a previous study, we showed that the photophysical parameters of a series of trans-(NHC)2Pt(CC-Ar)2 complexes vary strongly with emission energy; in general, the lifetime and emission quantum yield decreased with increasing emission energy.18 This trend is attributed to an increase in the nonradiative decay rate with emission energy. Due to this effect, we selected the complex IPtPCF3 from the previous study as a point of reference to compare with the photophysical parameters for IPt-MB and IPt-DB. 18,19 The photophysical parameters for IPtPCF3 are included in Table 2, and it can be seen that its emission energy is within 0.02 eV of the Br-substituted complexes. Comparison of the data in Table 2 reveals that the emission quantum yield, lifetime, and $k_{\rm r}$ and $k_{\rm nr}$ values for IPt-DB and IPtPCF3 are very similar, which suggests that photophysical parameters of the dibromo-substituted complex are "typical" for a -(NHC)₂Pt(CC-Ar)₂ complex. By contrast, the emission parameters of IPt-MB are clearly anomalous, with a much lower emission yield and shorter lifetime than reference IPtPCF₃. The anomalous behavior of IPt-MB can be attributed to a substantially larger non-radiative decay rate.

The photophysical properties of IPt-MB and IPt-DB in the solid-state were measured in poly(methyl methacrylate) (PMMA) matrices at 2 wt% complex loading. The matrices were fabricated by mixing the complexes with the methyl methacrylate monomer with a free radical initiator, pouring the mixture into a mold, and then heating in an oven at 75 °C for 48 h. The emission spectra and photophysical parameters were measured in the PMMA matrices and the spectra are shown in Fig. 2c and d and the photophysical parameters are compiled in Table 3. Both complexes feature blue emission that is slightly blue-shifted and broadened compared to solution, and with higher quantum efficiency. Interestingly, the emission yield of IPt-DB increased by ~2-fold in PMMA compared to the solution, whereas for IPt-MB the yield increased by more than 5-fold. The increases in emission yields are accompanied by increases in emission lifetimes. In both cases, the increased emission yields and lifetimes in the PMMA matrix are mainly due to a decrease in k_{nr} , and the decrease in

Table 3 Photophysical properties of IPt-MB and IPt-DB in PMMA

Compound	$\lambda_{\max}^{(\mathrm{em})}/$ nm	$\phi_{ m Ph/PMMA}$	$\langle \tau \rangle^a / \mu s$	$\frac{k_{\rm r}^{\ b}/10^4}{{ m s}^{-1}}$	$\frac{k_{\rm nr}^{\ \ b}}{{\rm s}^{-1}} / 10^4$	E _{em} (eV)
IPt-MB	451	0.11	26.6	0.41	3.35	2.74
IPt-DB	453	0.54	33.5	1.61	1.40	2.73
IPtPCF ₃ ^c	452	0.44	23	1.91	2.43	2.74
NPtPE1 ^c	444	0.30	9.0	3.33	7.78	2.79

^a The emission decays in PMMA were biexponential. Median lifetimes calculated by $\langle \tau \rangle = \alpha_1 \tau_1 + \alpha_2 \tau_2$, where $\alpha_1 \tau_1$ are the normalized amplitude and lifetime of the decay components. ^bCalculated using the equations: $k_{\rm r} = \Phi_{\rm PL}/\tau_{\rm PL}$ and $k_{\rm nr} = (1/\tau_{\rm PL}) - k_{\rm r}$, where $\tau_{\rm PL} = \langle \tau \rangle$. Data from ref. 19.

 $k_{\rm nr}$ is significantly larger for IPt-MB. Comparing the photophysical parameters for the IPt-MB and IPt-DB with the reference complex IPt-CF3 it is seen that the dibromo complex exhibits parameters that are very similar to the reference, whereas the non-radiative decay rate for IPt-MB is larger. Clearly for both complexes the decreased non-radiative decay rate in PMMA is associated with restricted motion that is available to the excited state complexes in the glassy polymer matrix. However, the fact that IPt-MB continues to exhibit a slightly larger non-radiative decay rate even in the solid state suggests that the mechanism that is responsible for accelerating the decay rate is still active to some extent in the polymer matrix.

Temperature-dependent emission of IPt-MB and IPt-DB were measured in 2-methyl tetrahydrofuran (MTHF) and the results are summarized in Fig. S12.† The emission of both complexes increased in intensity substantially at lower temperature, consistent with non-radiative decay occurring via a thermally activated process as has been observed for related (NHC)₂Pt(CC-Ar)₂ chromophores. ¹⁸ The emission undergoes a blue-shift below the solvent glass point (<120 K); similar effects have been seen in related complexes and have been attributed to emission from higher energy conformers that are unable to relax in the rigid medium. 18,41 Fig. S12c† compares the emission of the two complexes just above the solvent glass point; these spectra clearly display a vibronic progression at lower energies from the 0-0 band. Each complex displays vibronic bands at ~950, 1500 and 2050 cm⁻¹ which can be assigned to aryl C-H (out of plane), aryl C=C and acetylide C≡C stretches, respectively. The mid-frequency band (~1500 cm⁻¹) is distinctly different in intensity for the two complexes. While there are differences in the low temperature emission, there are not significant differences that could be attributed to vibronic coupling to the meta- or para-bromo substituents.

Density functional theory calculations

Density functional theory (DFT) and time-dependent DFT (TD-DFT) calculations were performed on the bromo-substituted platinum complexes using B3LYP functional in the gas phase. The full double zeta basis set, D95, was used for atoms C, H, N, and Br. 43 For Pt, a Stuttgart/Dresden effective core **Dalton Transactions** Paper

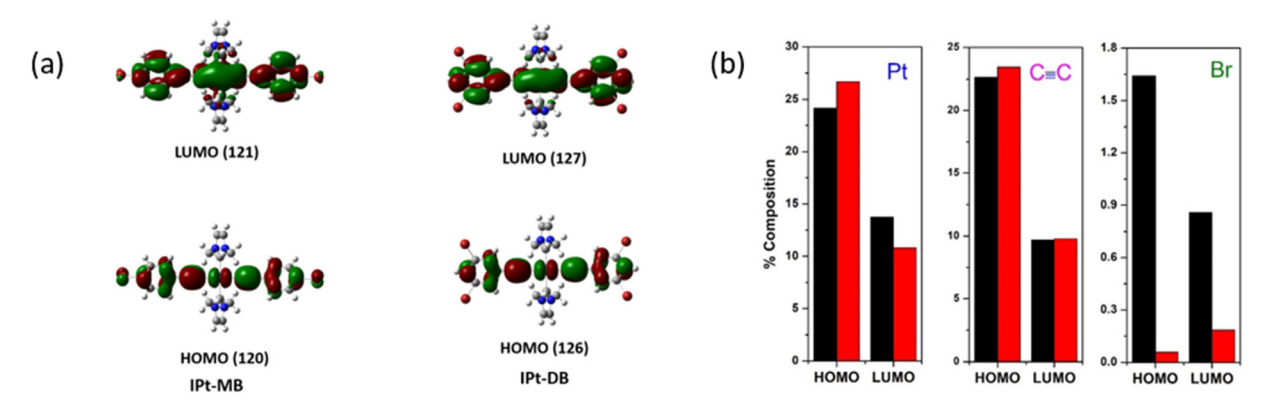


Fig. 3 (a) DFT optimized HOMO-LUMO orbitals of IPt-MB and IPt-DB. (b) Atomic orbital composition of HOMO and LUMO. IPt-MB (black), IPt-DB (red).

potential was used.44 The Cartesian coordinates for the optimized geometry of the complexes are provided in the ESI section.† The HOMO and LUMO orbital density plots for the geometry optimized ground state structures of both IPt-MB and IPt-DB are shown in Fig. 3a. Inspection of the orbital plots reveals that the HOMO and LUMO are localized on the platinum center and the two aryl acetylide ligands. Insight into the orbital basis for the complexes' near-UV absorption bands comes from the TD-DFT results that are shown in Tables S2 and S3 in the ESI section.† Here it is seen that the lowest energy transition is entirely comprised of the HOMO → LUMO transition. Given the distributions of the frontier orbitals (Fig. 3a), it is reasonable to conclude that the transition is mainly π - π *, with a small degree of metal-to-ligand charge transfer character.45 In addition to the ground-state and TD-DFT calculations, we also computed the energy and optimized geometry of the first triplet excited (T₁) state for IPt-MB and IPt-DB. The adiabatic triplet energy of the complexes was calculated from the difference between geometry-optimized energies of S₀ and T₁. 18 By using this approach, the triplet energy of IPt-MB and IPt-DB was computed as 2.76 and 2.91 eV, respectively. These energies correspond to phosphorescence wavelengths of 449 nm and 426 nm, which agree approximately with the experimental wavelengths of IPt-MB (456 nm) and IPt-DB (458 nm), respectively.

In order to understand the contributions of the -Br atoms to the frontier orbitals of IPt-MB and IPt-DB, an analysis was carried out to determine the atomic contributions to the HOMO and LUMO using the Mulliken method as implemented in Multiwfn 3.8 (Fig. 3b).^{46,47} For both complexes, the contribution of -Br localized orbitals to the HOMO and LUMO is relatively low (<2%). However, importantly the contribution of -Br orbitals for IPt-DB is much lower than for IPt-MB; indeed for IPt-DB the contribution of the two Br atoms to the HOMO and LUMO is nearly insignificant. This difference clearly results from the positional relationship of the -Br atoms in the two complexes (i.e., meta- vs. para-) relative to the Pt-CC-linkage. We conclude from this analysis that the effect of -Br on the lowest excited states is expected to be greater for

IPt-MB compared to IPt-DB due to the greater contribution of -Br to the frontier orbitals in the former. This is consistent with the experimental photophysical data, which show that **IPt-DB** is similar in properties to the reference complex (IPtPCF₃), while IPt-MB exhibits an anomalously large nonradiative decay rate.

Transient absorption spectroscopy

To gain insight into the excited state dynamics of the complexes, UV-visible femtosecond transient absorption (fsTA) experiments were carried out in THF, and the results are presented in Fig. 4. Overall, IPt-MB and IPt-DB show similar features in their excited state absorption. Upon excitation at 330 nm, both IPt-MB and IPt-DB reveal an instantaneous appearance of a broad excited state absorption (ESA) throughout the visible range, with a sharp peak around 650 nm. This band continues to rise for approximately 20 ps and the peak absorption shifts slightly to longer wavelength. Kinetic analysis of the TA reveals that the absorption rise seen at early delay times is distinctly slower for IPt-DB compared to IPt-MB (4.7 ps and 8.4 ps, respectively, see Fig. 4c). Previously reported fsTA studies on a series of trans-(NHC)2Pt(CC-Ar)2 complexes show very similar TA spectra and dynamics as seen for IPt-MB and IPt-DB.²¹ In the previous work, the TA has been attributed to the triplet excited state that is produced in <1 ps by ultrafast intersystem crossing. The process that takes place on the 1-20 ps timescale that causes the "rise" has been attributed to a geometric relaxation involving torsion of the arylene groups.21 This process occurs because in the triplet state, there is a shallow energy minimum that favors the conformation where the arylene rings are in the same plane as the PtC4 plane. Interestingly, the slower dynamics are observed for the di-substituted IPt-DB complex, and this may be due to the slower arylene ring torsion arising from the interaction of the two meta-Br atoms with the solvent environment (e.g. solvent friction).48

General discussion

The primary objective of this study was to explore the effect of the introduction of Br substituents onto the arylacetylene groups on the photophysics of trans-(NHC)₂Pt(CC-Ar)₂ comPaper Dalton Transactions

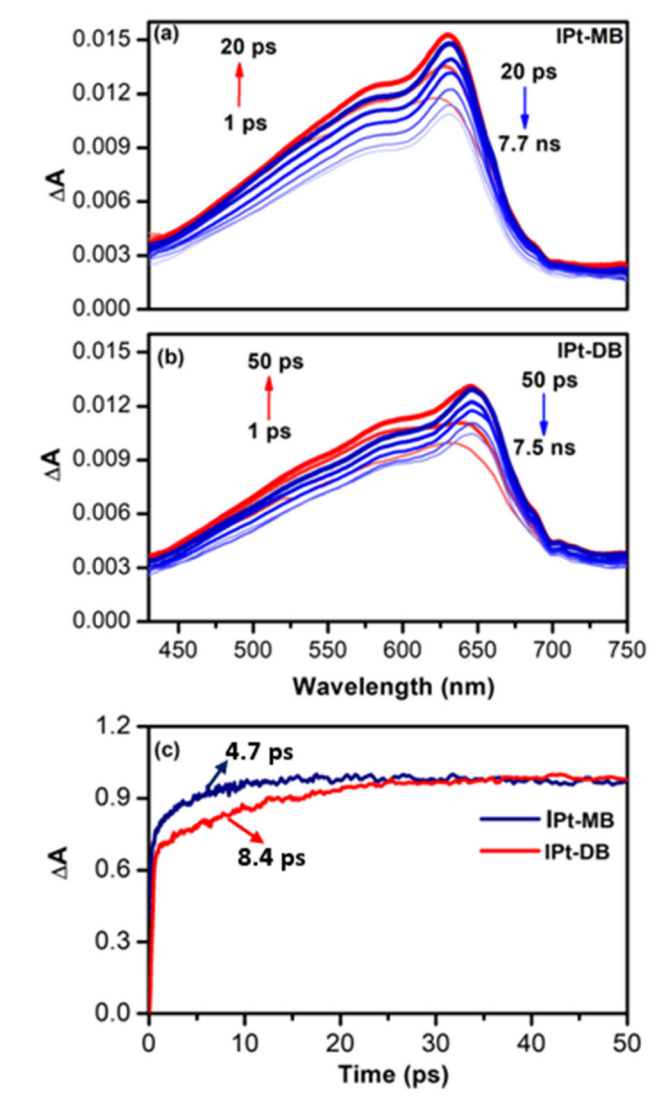


Fig. 4 Femtosecond transient absorption of IPt-MB (a) and IPt-DB (b) in THF with excitation of 330 nm (100 μ J). (c) Kinetic traces of IPt-MB (blue) and IPt-DB (red). Labels indicate the exponential lifetime of the slow transient absorption "rise". Lifetimes determined by global kinetic analysis (see ESI Fig. S15†).

plexes. The goal was to increase the triplet decay rate but maintain a high phosphorescence yield by enhancing both the rates of radiative and non-radiative decay. Previous work on the photophysics of aromatic hydrocarbons has found that Br can exert a substantial effect on the rate of intersystem crossing, and the rates of radiative and non-radiative decay of triplet states. We hypothesized that similar effects might be exerted by Br-substitution in the *trans*-(NHC)₂Pt(CC-Ar)₂ complexes. In addition, the previous work has found that the effect of Br-substitution is strongly dependent on the position of the substituents, due to the positional dependence of the atom's effect on mixing the singlet and triplet wavefunctions. ³⁴

To address the hypothesis regarding Br-substitution, the complexes **IPt-MB** and **IPt-DB** were designed and synthesized. In **IPt-MB**, the Br-is located *para*-relative to the Pt-CC-unit,

whereas in **IPt-DB** the two Br-atoms are both located *meta*-relative to the Pt-CC-unit. The DFT calculations indicate that the *para*-Br in **IPt-MB** contributes to the HOMO and LUMO which are the predominant levels involved in the transitions to the lowest excited state. By contrast, the *meta*-Br-atoms in **IPt-DB** contribute very little to the frontier orbitals. Given this result, it is unsurprising that the photophysical parameters of **IPt-DB** are hardly affected by the Br-substituents whereas the parameters are significantly affected in **IPt-MB**.

The results of the photophysical studies of IPt-MB in solution and the PMMA polymer matrix reveal that the para-Br substituent leads to a substantial increase in the non-radiative decay rate in solution and a smaller, albeit noticeable, increase in non-radiative decay rate in the polymer matrix. By contrast, systematic changes in the radiative decay rate of IPt-MB in solution and in the polymer matrix relative to the other complexes are not as clear. If the para-Br is acting to increase the rates of the spin-forbidden transition (triplet to singlet decay) in IPt-MB, we would expect the effect to be reflected by commensurate increases in both the radiative and non-radiative decay rates. Given that the primary effect seems to be in the non-radiative decay rate, we conclude that the effect of para-Br substitution is not due to enhanced spin-orbit coupling, but rather due to the introduction of a new non-radiative decay channel, via vibronic coupling with a low frequency vibrational mode (e.g., C-Br stretch or bend). This conclusion is supported by the fact that the non-radiative decay rate of IPt-MB decreases in the polymer matrix, where vibrational modes with relatively large displacement would be suppressed.

One hypothesis that we considered is that if non-radiative decay is strongly coupled to the C(Ar)-Br stretch, excited state decay could activate homolysis of the C-Br bond. To probe whether this is occurring, we carried out long term photolysis of **IPt-MB** in outgassed solution with 313 nm excitation; however, this experiment did not lead to noticeable photodegradation of the complex. While this does not disprove that the non-radiative decay is coupled to a C-Br vibrational mode, it does show that the complex is not subject to photochemical degradation induced by photolysis.

In summary, the effects of Br-substitution are strongly positional dependent. The two Br-atoms that are located *meta*-exert little influence on the photophysical properties of the complex relative to the reference. By contrast, the single Br-atom that is located *para*-exerts a strong effect on the complexes' photophysics by enhancing the non-radiative decay rate. However, since there is little effect on the radiative decay rate, the Br-substituent leads to an overall decrease in the emission quantum efficiency in **IPt-MB**, which from the stand-point of application is a disappointing result.

Conclusion

This study reports the synthesis and photophysical characterization of two novel complexes, **IPt-MB** and **IPt-DB**, with the general structure *trans*-(NHC)₂Pt(CC-Ar)₂. **IPt-MB** features one

Dalton Transactions Paper

para-substituted Br atom on the aryl acetylide ligands, while IPt-DB features two meta-substituted Br atoms on the aryl acetylides. It was hypothesized that inclusion of the Br atoms would enhance spin-orbit coupling via the heavy atom effect, influencing the radiative and non-radiative decay rates. IPt-MB and IPt-DB both display sky blue emission in solution and in PMMA matrix. IPt-DB features photophysical properties that are similar to benchmark trans-(NHC)₂Pt(CC-Ar)₂ chromophores. By contrast, IPt-MB exhibits a substantially lower emission quantum vield and shorter lifetime in solution due to an enhanced rate of non-radiative decay. Analysis of the results in the context of DFT and TD-DFT calculations suggests that the enhanced non-radiative decay rate of IPt-MB is due to coupling of the excited state decay with a low-frequency vibrational mode associated with the para-Br substituents. This study enhances our understanding of structural effects on the luminescence properties of trans-(NHC)₂Pt(CC-Ar)₂ complexes, some of which have demonstrated promising performance as phosphors for deep blue OLEDs.

Conflicts of interest

There are no conflicts to declare.

Acknowledgements

This work was supported by the National Science Foundation (grant CHE-1904288).

References

- 1 W.-Y. Wong and P. D. Harvey, *Macromol. Rapid Commun.*, 2010, 31, 671–713.
- X. Zhang, Y. Hou, X. Xiao, X. Chen, M. Hu, X. Geng,
 Z. Wang and J. Zhao, *Coord. Chem. Rev.*, 2020, 417, 213371.
- 3 H. Yersin, A. F. Rausch, R. Czerwieniec, T. Hofbeck and T. Fischer, *Coord. Chem. Rev.*, 2011, 255, 2622–2652.
- 4 G. Baryshnikov, B. Minaev and H. Ågren, *Chem. Rev.*, 2017, 117, 6500–6537.
- 5 L. Mercs and M. Albrecht, *Chem. Soc. Rev.*, 2010, 39, 1903–1912.
- 6 R. Visbal and M. C. Gimeno, *Chem. Soc. Rev.*, 2014, 43, 3551-3574.
- 7 T. Ogawa, W. M. C. Sameera, D. Saito, M. Yoshida, A. Kobayashi and M. Kato, *Inorg. Chem.*, 2018, 57, 14086– 14096.
- 8 K. Li, G. S. Ming Tong, Q. Wan, G. Cheng, W.-Y. Tong, W.-H. Ang, W.-L. Kwong and C.-M. Che, *Chem. Sci.*, 2016, 7, 1653–1673.
- 9 Y. Zhang, O. Blacque and K. Venkatesan, *Chem. Eur. J.*, 2013, **19**, 15689–15701.
- 10 I. Omae, Coord. Chem. Rev., 2016, 310, 154-169.
- 11 Q.-X. Liu, F.-B. Xu, Q.-S. Li, H.-B. Song and Z.-Z. Zhang, *Organometallics*, 2004, 23, 610–614.

- 12 T. Strassner, Acc. Chem. Res., 2016, 49, 2680-2689.
- 13 S. Stipurin and T. Strassner, *Eur. J. Inorg. Chem.*, 2021, 804–813.
- 14 Y. Zhang, J. A. Garg, C. Michelin, T. Fox, O. Blacque and K. Venkatesan, *Inorg. Chem.*, 2011, 50, 1220–1228.
- 15 Y. Zhang, J. Clavadetscher, M. Bachmann, O. Blacque and K. Venkatesan, *Inorg. Chem.*, 2014, 53, 756–771.
- 16 T. Maganti and K. Venkatesan, ChemPlusChem, 2022, 87, e202200014.
- 17 R. W. Winkel, G. G. Dubinina, K. A. Abboud and K. S. Schanze, *Dalton Trans.*, 2014, 43, 17712–17720.
- 18 J. D. Bullock, S. R. Valandro, A. N. Sulicz, C. J. Zeman, K. A. Abboud and K. S. Schanze, *J. Phys. Chem. A*, 2019, 123, 9069–9078.
- 19 J. D. Bullock, Z. Xu, S. Valandro, M. Younus, J. Xue and K. S. Schanze, ACS Appl. Electron. Mater., 2020, 2, 1026– 1034.
- 20 R. He, Z. Xu, S. Valandro, H. D. Arman, J. Xue and K. S. Schanze, ACS Appl. Mater. Interfaces, 2021, 13, 5327– 5337.
- 21 S. R. Valandro, R. He, J. D. Bullock, H. Arman and K. S. Schanze, *Inorg. Chem.*, 2021, 60, 10065–10074.
- 22 G. Hong, X. Gan, C. Leonhardt, Z. Zhang, J. Seibert, J. M. Busch and S. Bräse, *Adv. Mater.*, 2021, 33, 2005630.
- 23 J. Lee, H.-F. Chen, T. Batagoda, C. Coburn, P. I. Djurovich, M. E. Thompson and S. R. Forrest, *Nat. Mater.*, 2016, 15, 92–98.
- 24 Y. Im, S. Y. Byun, J. H. Kim, D. R. Lee, C. S. Oh, K. S. Yook and J. Y. Lee, *Adv. Funct. Mater.*, 2017, 27, 1603007.
- 25 A. K. Pal, S. Krotkus, M. Fontani, C. F. R. Mackenzie, D. B. Cordes, A. M. Z. Slawin, I. D. W. Samuel and E. Zysman-Colman, Adv. Mater., 2018, 30, 1804231.
- 26 R. Hamze, S. Shi, S. C. Kapper, D. S. Muthiah Ravinson, L. Estergreen, M.-C. Jung, A. C. Tadle, R. Haiges, P. I. Djurovich, J. L. Peltier, R. Jazzar, G. Bertrand, S. E. Bradforth and M. E. Thompson, *J. Am. Chem. Soc.*, 2019, 141, 8616–8626.
- 27 J.-H. Lee, C.-H. Chen, P.-H. Lee, H.-Y. Lin, M.-k. Leung, T.-L. Chiu and C.-F. Lin, *J. Mater. Chem. C*, 2019, 7, 5874–5888.
- 28 Y. Wu, Z. Wen, J. I. C. Wu and T. S. Teets, *Chem. Eur. J.*, 2020, 26, 16028–16035.
- 29 A. Maheshwaran, V. G. Sree, H.-Y. Park, H. Kim, S. H. Han, J. Y. Lee and S.-H. Jin, *Adv. Funct. Mater.*, 2018, **28**, 1802945.
- 30 A. Monkman, ACS Appl. Mater. Interfaces, 2022, 14, 20463-20467.
- 31 H. van Eersel, P. A. Bobbert, R. A. J. Janssen and R. Coehoorn, *Appl. Phys. Lett.*, 2014, **105**, 143303.
- 32 J. D. Bullock, A. Salehi, C. J. Zeman, K. A. Abboud, F. So and K. S. Schanze, ACS Appl. Mater. Interfaces, 2017, 9, 41111-41114.
- 33 M. A. El-Sayed, Acc. Chem. Res., 1968, 1, 8-16.
- 34 J. C. Miller, J. S. Meek and S. J. Strickler, *J. Am. Chem. Soc.*, 1977, **99**, 8175–8179.
- 35 S. Gan, S. Hu, X.-L. Li, J. Zeng, D. Zhang, T. Huang, W. Luo, Z. Zhao, L. Duan, S.-J. Su and B. Z. Tang, ACS Appl. Mater. Interfaces, 2018, 10, 17327–17334.

Paper

36 Kenry, C. Chen and B. Liu, Nat. Commun., 2019, 10, 2111.

- 37 R. Makhoul, J. B. G. Gluyas, K. B. Vincent, H. Sahnoune, J.-F. Halet, P. J. Low, J.-R. Hamon and C. Lapinte, *Organometallics*, 2018, 37, 4156–4171.
- 38 J. Wang, J. Li, T. Aoki, T. Kaneko, M. Teraguchi, Z. Shi and H. Jia, *Macromolecules*, 2017, **50**, 7121–7136.
- 39 K. Sonogashira, T. Yatake, Y. Tohda, S. Takahashi and N. Hagihara, *J. Chem. Soc., Chem. Commun.*, 1977, 291–292.
- 40 K. Sonogashira, Y. Fujikura, T. Yatake, N. Toyoshima, S. Takahashi and N. Hagihara, *J. Organomet. Chem.*, 1978, 145, 101–108.
- 41 K. Glusac, M. E. Köse, H. Jiang and K. S. Schanze, *J. Phys. Chem. B*, 2007, **111**, 929–940.

- 42 E. R. Batista and R. L. Martin, J. Phys. Chem. A, 2005, 109, 9856–9859.
- 43 T. H. Dunning and P. J. Hay, in *Modern Theoretical Chemistry*, ed. H. F. Schaefer, Springer, 1977, vol. 3, pp. 1–28.
- 44 D. Andrae, U. Häußermann, M. Dolg, H. Stoll and H. Preuß, *Theor. Chim. Acta*, 1990, 77, 123–141.
- 45 T. M. Cooper, D. M. Krein, A. R. Burke, D. G. McLean, J. E. Rogers and J. E. Slagle, *J. Phys. Chem. A*, 2006, **110**, 13370–13378.
- 46 T. Lu and F. Chen, J. Comput. Chem., 2012, 33, 580-592.
- 47 T. Lu and F.-W. Chen, Acta Chim. Sin., 2011, 69, 2393-2406.
- 48 S. H. Courtney and G. R. Fleming, *J. Chem. Phys.*, 1985, **83**, 215–222.